Direct measurement of bending conformations in triatomic dihydride ions

T. Graber* and E. P. Kanter

Physics Division, Argonne National Laboratory, Argonne, Illinois 60439

J. Levin, D. Zajfman, and Z. Vager†

Department of Particle Physics, Weizmann Institute of Science, Rehovot 76 100, Israel

R. Naaman

Department of Chemical Physics, Weizmann Institute of Science, Rehovot 76 100, Israel

(Received 29 January 1997)

The distributions of bond angles in the triatomic dihydride ion series CH_2^+, NH_2^+, and H_2O^+ have been studied using the Coulomb explosion imaging method. These distributions were measured as a function of the cooling of the internal degrees of freedom of these ions. The distribution for the coldest sample of CH_2^+ molecules shows the most probable structure to be bent with substantial tunneling through the linear conformation. The most probable geometry for NH_2^+ was found to be linear, though the angular distribution is significantly different from a shape of a harmonic-oscillator ground-state prediction. In the case of H_2O^+, we find a bent structure as expected from theory. Evidence for a linear excited state in H_2O^+ is seen in the hotter distributions. Comparison to the adiabatic theoretical predictions shows good agreement with the most probable geometries. However, the measured distributions are systematically wider than the squared vibronic wave functions derived from the corresponding potential-energy surfaces. [S1050-2947(97)05308-0]

PACS number(s): 33.15.Bh, 33.15.Dj, 33.15.Hp, 39.90.+d

I. INTRODUCTION

Most of our existing experimental knowledge of gas-phase molecular structure comes from various gas-phase spectroscopic methods which measure differences between eigenvalues. The nuclear geometry is then fitted to these measured eigenvalue separations using a model Hamiltonian. This traditional and highly successful method is the basis of most of our understanding of the structures of small polyatomic molecules. It is believed to be especially accurate for rigid molecules, where the model predicts only minimal nuclear excursions from the fitted equilibrium geometries. A different approach to the experimental study of molecular structure is the Coulomb explosion imaging (CEI) technique, which samples the nuclear distribution within small molecules [1] and is particularly sensitive to molecular states exhibiting large-amplitude nuclear displacements from equilibrium.

In an ideal CEI experiment, the binding molecular electrons are instantly (on a time scale which is short compared to characteristic nuclear motions) stripped away, leaving a group of positively charged atomic fragments. The potential energy stored in this highly charged system is rapidly converted to kinetic energy of the fragments which move in a Coulomb interaction potential. By simultaneously measuring the asymptotic velocity of each molecular fragment, the original nuclear configuration of the molecule at the instant before the electrons were stripped can be deduced. This is a direct and model-independent method which yields the fully correlated many-body nuclear density distribution in an ensemble of molecules. While such experiments are generally insensitive to eigenvalues, those distributions are instead directly related to eigenfunctions, and thus provide a complementary source of molecular structure information. It is thus interesting to question the compatibility of these two approaches, namely, the spectroscopic method and the CEI method to molecular structure. In an effort to address this question directly, we have investigated the bending degree of freedom within several triatomic dihydride ions.

Triatomic molecules with relatively low potential barriers to linearity provide an excellent opportunity to study large-amplitude vibrations. Such ''quasilinear'' systems have been challenging to experimental and theoretical techniques alike. This is particularly evident when the bending amplitude becomes so large that no choice of coordinate systems allows simple separability of motions which is central to conventional descriptions of molecular vibrations. The series of light dihydride ions (CH_2^+, NH_2^+, H_2O^+) provides a particularly interesting test of such phenomena since, in their ground states, they span the range of bending motions from the fairly rigid H_2O^+, for which there have been numerous spectroscopic studies, to the floppy and lesser-known NH_2^+. In this work, we report results of CEI measurements of these molecules which demonstrate the diversity of such quasilinear bending motions, and compare to both spectroscopic data and theory. In Sec. II, we will review the predictions of *ab initio* theories for the ground-state structures of these dihydride molecular ions as well as existing experimental results.

II. DIHYDRIDE IONS

The experimental results and the theoretical predictions on the structure of H_2O^+, CH_2^+ and NH_2^+ in their electronic and vibrational ground state are summarized in Table I.

---

*Present address: Advanced Photon Source, Argonne National Laboratory, Argonne, IL 60439.

†Also at Physics Division, Argonne National Laboratory, Argonne, IL 60439.

TABLE I. Geometrical parameters and fundamental frequencies of the molecular ions: H_2O^+, CH_2^+, and NH_2^+ in their electronic ground states. A review of previous theoretical and experimental results (separated by a line—theoretical results are above the line) is given. The bond lengths are in Å, the angles in degrees, and energies in cm^{-1}. E_b is the energy barrier to linearity.

			H_2O^+ X^2B_1			
Ref.	r_e [r_0]	θ_e [θ_0]	E_b	ν_1	ν_2	ν_3
[15]	0.982	112.4		3887	1582	3979
[16] [a]	1.0074	108.5		3388	1518	3469
[17]	1.010	108.8	9187		1408	
[50]	0.997	109.1				
[20]	1.0004 [1.0003]	109.07 [110.22]		3380.6	1476.6	3436.3
[19]	1.010	108.9	8235	3350	1435	3400
[4]	0.9992	109.3	7886	3216	1412	3262
[5]				3200(50)	1380(50)	
[51]				3220(40)	1370(40)	
[18]	[0.9988]	[110.46]			1408	
[12]				3270.6(4.0)	1433.7(4.0)	
[52]	[1.006(7)]	[109.8(1.6)]				
[9]	1.001 [0.9898]	108.9 [111.0]		3213.00(9)		3259.031(3)
[10]					1431.198	
[53]	1.00(4)	108.4(5)			1370(100)	
[54]	0.9992(6)	109.30(10)		3212.860(3)		3259.036(2)
[13]				3182.7	1401.7	3219.5

			CH_2^+ X^2A_1			
Ref.	r_e	θ_e	E_b	ν_1	ν_2	ν_3
[23] [b]	1.083	137.9	998	2998.8	938.1	3268.9
[26]				2901	948	3118
[25]	1.08	138.7		2901	949	3118
[27]	1.094	140.8	1180	2934	1033	3324
[21]						3131.373(14)
[22]		144.6(3)				

			NH_2^+ X^3B_1			
Ref.	r_e	θ_e	E_b	ν_1	ν_2	ν_3
[26]				3330	792	3593
[31]		149.6	390		318 [c]	
[32]	1.0338	153.17	209	3118	918	3363
[33]	1.030	153.78	155	3052.3	847.9	3360
[28]					840(50)	
[29]	[1.029] [d]	[165] [d]				3359.9317(20)

[a]The results of the MCSCF-CI procedure.
[b]Based on Ref. [24].
[c]Zero vibrational level for the bending frequency.
[d]Based on the assumption of a rigid rotor and neglecting the inertial defect.

A. H_2O^+

Theory predicts that the ground-state electronic configuration for H_2O^+ correlates with a doubly degenerate linear $^2\Pi_u$ state. The Renner-Teller effect couples the electronic angular momentum to the vibrational angular momentum. This coupling causes a well-known breakdown of the Born-Oppenheimer approximation, since the electronic and vibrational motions can no longer be treated independently. The degenerate linear state splits into two potential-energy surfaces in which the ground state becomes bent $\bar{X}^2B_1$. The
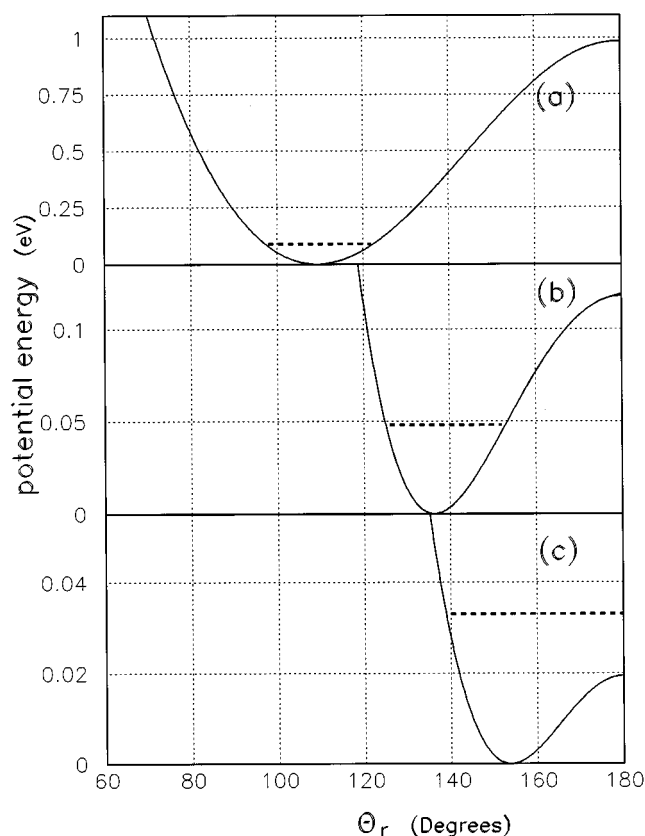
FIG. 1. Theoretical bending potentials for (a) H_2O^+ [4], (b) CH_2^+ [23], and (c) NH_2^+ [33]. The dashed lines represent the energy of the vibrational ground states.

first excited state $\widetilde{A}^2A_1$ remains linear. The barrier where these surfaces meet is ~ 1 eV higher than the ground-state minimum [see Fig. 1(a)].

The H_2O^+ cation plays an important role in astrophysics. It has been observed in several comet tails [2] and in the interstellar media [3]. It has been extensively studied both theoretically and experimentally. We shall mainly review the previous work that has relevance to the ground-state structure, though a more complete literature survey can be found in Ref. [4]. H_2O^+ was first observed spectroscopically in a photoelectron study by Brundle and Turner [5] in 1968. In 1976, analysis of the high-resolution spectrum lead to its identification as one of the key constituents of the tail of Comet Kohoutek [6,7,2]. More recently, high-resolution spectroscopic measurements have probed rovibrational transitions near the ground electronic state [8–11]. Reutt *et al.* [12] obtained spectroscopic constants of the $\widetilde{X}^2B_1$ and $\widetilde{A}^2A_1$ excited state by photoelectron spectroscopy. Forney, Jacox, and Thompson [13] studied the vibrational fundamentals of H_2O^+ (and isotope substituted) ions trapped in a solid neon matrix.

The CEI technique was applied by Zajfman *et al.* [14] to study the bond angle distribution. The H_2O^+ ions were created by electron impact on water vapor. The resulting distribution showed evidence of a mixture of both a bent and a linear structure (see [14]). After subtracting a smooth background, assumed to be due to the contribution of the linear state, the data were analyzed in the harmonic approximation

and the equilibrium angle was found to be in good agreement with other measurements and theoretical predictions. In the experiment reported here, a source of cold molecular ions has been used and, indeed, this contribution from the linear structure no longer appears.

The modern theoretical studies of H_2O^+ start with Smith, Jørgensen, and Öhrn [15], Fortune, Rosenberg, and Wahl [16], and the classical paper by Jungen and Merer [17], who included Renner-Teller coupling in their derivation of the $\widetilde{X}^2B_1$ and $\widetilde{A}^2A_1$ effective bending potentials based on the emission spectrum measured by Lew [18]. More recently *ab initio* derivations of such potentials were presented [19,20] and the latest calculation of the $\widetilde{X}^2B_1$ energy surface by Brommer *et al.* [4] shows a significant modification of the derivation by Jungen and Merer [17], especially near the linear conformation. In fact, the barrier to linearity was found to be lower by 1301 cm^{-1} than the earlier result.

B. CH_2^+

The cation CH_2^+ is another example of a Renner-Teller molecule. The degeneracy of the $^2\Pi_u$ electronic ground state in CH_2^+ is removed by vibronic coupling, producing the bent $\widetilde{X}^2A_1$ ground state and the linear $\widetilde{A}^2B_1$ first excited state. All recent *ab initio* treatments agree that the bent $\widetilde{X}^2A_1$ ground-state potential has a very low barrier at the linear conformation [~ 1000 cm^{-1}; see Fig. 1(b)]. It is smaller by a factor of ~ 10 than the barrier in H_2O^+. Such a low barrier would allow a finite linear amplitude in the vibrational ground state. It is therefore classified as a quasilinear system.

The infrared spectrum of CH_2^+ has been studied experimentally by Rösslein *et al.* [21]. So far this is the only published spectrum of this molecular ion. They were able to measure transitions of the antisymmetric ν_3 band of CH_2^+ and reported $\nu_0 = 3131.337(14)$ cm^{-1}. They concluded that the measured spectrum could be fitted equally well either by a linear or by a bent structure. Our group has previously reported the bond angle distribution for CH_2^+, measured using the CEI technique [22]. In Ref. [22], we demonstrated conclusively that the molecule CH_2^+ has a bent structure in the ground state.

Carter and Handy [23] studied theoretically the rovibrational levels of the Renner-Teller coupled $\widetilde{X}^2A_1$ and $\widetilde{A}^2B_1$ states. They used the ground-state potential surface from *ab initio* calculations by Bartholomae, Martin, and Sutcliffe [24], who predicted $r_e = 1.105$ Å and an equilibrium angle of $\theta_e = 137.9°$. Pople and Curtiss [25] determined the equilibrium structure of CH_2^+ at the HF/6-31G* level of theory, and reported a bent structure with $r_e = 1.080$ Å and $\theta_e = 138.7°$. Vibrational frequencies were also calculated and after scaling by 0.89 were found to be $\nu_1 = 2901$ cm^{-1}, $\nu_2 = 949$ cm^{-1}, and $\nu_3 = 3118$ cm^{-1}. These frequencies are in agreement with those previously calculated by DeFrees and McLean [26]. Recently Reuter and Peyerimhoff [27] recalculated the potential surfaces and vibronic levels of both ground and excited electronic states. They reported $r_e = 1.094$ Å and $\theta_e = 140.8°$ for the structure of the ground state.

C. NH_2^+

The molecular ion NH_2^+, which is isoelectronic with CH_2, is another example of a molecule which is expected to exhibit quasilinear behavior. However, unlike the other two molecules considered, NH_2^+ has a triplet $\widetilde{X}^3B_1$ electronic ground state which correlates to a nondegenerate linear state $^3\Sigma_g^-$, and thus is not a Renner-Teller-type molecule. Like CH_2^+, however, it is expected to have a very low barrier at the linear conformation. For quasilinear molecules such as CH_2^+ and NH_2^+, it is generally difficult to distinguish spectroscopically between the linear and bent ground state structures.

Photoelectron studies of NH_2 by Dunlavey et al. [28] found that the minimum of the $\widetilde{X}^3B_1$ ground-state potential and the minimum of the $\widetilde{a}^1A_1$ first excited state of NH_2^+ were separated by 0.99 ± 0.02 eV. They were also able to extract the bending vibrational frequency and found that $\nu_2 = 840 \pm 5$ cm^{-1}. Recently Okumura et al. [29] and Kabbadj et al. [30] used a frequency difference laser spectroscopic technique to study absorption in the 2900–3500 –cm^{-1} region. They observed four hot bands as well as the ν_3 fundamental band. As in the case of CH_2^+, they pointed out that the spectrum they measured could be fitted equally well by a linear or an asymmetric rotor Hamiltonian, and that the large-amplitude bending vibrations prevented them from experimentally determining the molecular structure.

In 1979 Peyerimhoff and Buenker [31] reported on an *ab initio* study in which the potential energy surfaces for the low-lying bending states of NH_2^+ were calculated using a multireference double configuration-interaction algorithm. They found that the $\widetilde{X}^3B_1$ electronic ground state was bent with an angle of $\theta_0 = 149.6°$. The barrier at the linear conformation for this potential surface was determined to be 390 cm^{-1}. The zero-point vibrational energy of the bending mode was given as 318 cm^{-1}, which is below the barrier at the linear conformation. This would lead to a maximum in the ground-state vibrational wave function at an angle that is smaller than 180°, as is the case for CH_2^+. In the same paper, they also reported on the first two excited singlet states. The $\widetilde{a}^1A_1$ was found to have a minimum at $\theta_0 = 107.6°$ at an energy of 1.29 eV above the $\widetilde{X}^3B_1$ ground state. This separation energy is slightly larger than the value 0.99 ± 0.02 eV found by Dunlavey et al. [28]. The $\widetilde{b}^1B_1$ state was found to have a minimum at $\theta_0 = 155.2°$ at an energy of 2.03 eV above the ground state. Jensen, Bunker, and McLean [32] predicted the barrier at the linear conformation of the $\widetilde{X}^3B_1$ ground state potential surface to be 209 cm^{-1}. They also obtained $r_e = 1.0338$ Å and $\theta_e = 153.17°$ for the bond-length and bond-angle equilibrium values. They determined the zero-point energy of the ν_2 band to be 290 cm^{-1}. It should be stressed that, for this more recent calculation, the zero-point energy lies above the barrier at the linear conformation [see Fig. 1(c)]. This would lead to a very flat maximum in the ground vibrational state wave function that would peak at an angle of 180°. The recent calculation of the ground-state potential surface in Ref. [33], based on experimentally observed transitions, predicted an even lower barrier at the linear conformation (155 cm^{-1}). The equilibrium values for the bond length and angle are in agreement with Ref. [32].

III. EXPERIMENT

Molecular structure parameters can be determined accurately by the CEI technique when the molecule studied is prepared in a well-defined state. In earlier CEI experiments the development of a general method to prepare a molecular ion in its ground vibrational state presented a technical challenge. For example, in an experiment which measured the geometry of C_3^+ [34], it was determined that the equilibrium structure of the molecule deduced from the data might depend sensitively on the vibrational temperature of the ensemble of molecules studied [35]. In those measurements, a duoplasmatron source had been modified to produce ionization by low-energy electron impact in a low-pressure gas [36]. By adjusting the electron energy so that it was near the threshold for ionization, it was hoped that it would produce relatively cold molecules. This method, however, is limited in general to molecules where the daughter ions are structurally similar to the parent neutrals as, for example, the case of H_2O^+ [14].

In general, the conventional ion sources employed in nuclear accelerators produce vibrationally ''hot'' molecular ions [37,38]. To alleviate the ''hot'' distribution problem, a new type of ion source was developed for use in the 5-MV Argonne Dynamitron. This source utilizes the principle of vibrational cooling by supersonic expansion [39]. The cation He_2^+ was used as an initial test case for this source. In Refs. [39,40], it was demonstrated that this supersonic expansion source produced vibrationally cold He_2^+ ions. Since this ion source has been in operation, we have studied many additional diatomic and polyatomic molecular ions, and in all cases have observed significant vibrational cooling. A subsequent improvement in the source was the shielding of the expansion region from electrostatic fields. These fields, which were associated with the electron gun, caused the molecular ions to accelerate relative to neutral particles in the expansion. The ions would then make relatively high-energy collisions with the other constituents in the expansion. The energy transfer in these collisions was in some cases sufficient to cause vibrational excitation. There are several experimental examples of molecular ions that show this type of collisional heating in the data presented here. But, for all the measured species, we also present results for the best cooling conditions of the improved cold source.

The experiment begins with a dihydride molecular ion being created in the cold source and then accelerated to energies ≥ 250 keV/amu by the Argonne 5-MV Dynamitron (see Fig. 2). To insure the proper charge to mass ratio, two bending magnets are used to mass analyze the beam and steer it to the CEI beam line. Collimators along the beam line limit the beam divergence to less than 0.17 mrad (full width at half maximum). After collimation, the beam enters a scattering chamber where it is electrostatically pre-deflected to purge it of any contaminants, such as fragments of molecules that have dissociated during flight. After passing through the pre-deflectors, the molecule is stripped of its valence electrons by an ultrathin Formvar target (~ 100 Å or less [41]).
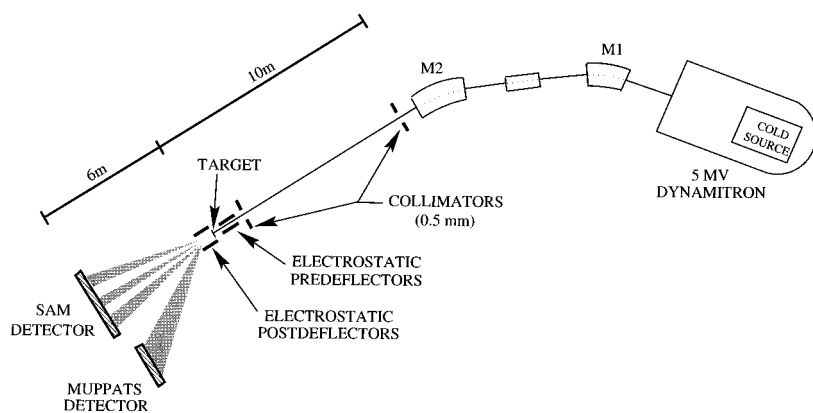
FIG. 2. A schematic view of the experimental setup (see text).

The time for single electron loss is of the order of 10^{-17} s. Thus, within less than 10^{-16} s all the binding electrons are stripped, and the Coulomb repulsion process starts. This time is short compared to the typical nuclear motions (vibrational and rotational). It is also two orders of magnitude less than the stripping time of electrons by a state of the art pulsed laser [42].

During beam tuning for each experiment, an energy sensitive surface barrier detector was used as a diagnostic aid for rapid identification of molecular species. It was insertable into the beam path after the target and provided a mass spectrum of the molecular fragments. This enabled an unambiguous identification of the molecules within the beam.

Downstream of the target, at a distance of ~ 6 m, two large-area multiwire position and time sensitive detectors (MUPPATS [43] and SAM [44]) detected the fragment ions in triple coincidence. In this experiment, fragments from the XH_2^+ molecules were post-deflected so that the light ions H^+ were directed toward MUPPATS, and heavy ions X^{n+} (where $n=1,2,3,4,\ldots$) were directed toward SAM. Post-deflection not only directs the beam to the proper detector, it also spatially separates the charge states of the heavy ion on the surface of the SAM detector. This allows the analysis of each event according to the charge state of the heavy ion.

From the position and relative time measurements, the final velocity vector is extracted for each fragment. In the case of the XH_2^+ molecules, we transform the velocities from the laboratory frame of reference to a frame in which the heavy ion (X) is located at the origin. A ''velocity-space'' (V-space) bond angle θ_v, which is the angle between the two proton velocity vectors measured relative to the heavy ion, is then extracted from the data.

A. *R*-space analysis

For obtuse bond angles, the V-space angle θ_v is closely related to the more familiar internal coordinate (R-space) bond angle θ_r. A typical example is given in Fig. 3, where the mapping of $\cos\theta_r$ to $\cos\theta_v$ in the case of an ideal Coulomb explosion (i.e., pure Coulombic repulsion and no target effects) of NH_2^+ is shown. The line $\cos\theta_v = \cos\theta_r$ has been added for comparison. For small R-space angles the proton-proton repulsion dominates the Coulomb explosion giving a much larger V-space angle θ_v. However, for the region where $\theta_r > 100°$, the proton-proton interaction is relatively weak, and the difference between θ_r and θ_v is quite small.

Therefore, for quasilinear molecules (such as CH_2^+ and NH_2^+), θ_v is a good zero-order approximation for θ_r. This allows an intuitive impression of the final results by inspection of the raw angular distribution data. In any case, for bend angles $\theta_r > 50°$ a unique interpretation of the data is possible.

In order to allow for a quantitative structural interpretation of the CEI results and deconvolution of experimental smearing effects, a Monte Carlo simulation of the CEI experiment has been developed [45,46]. The simulation takes into account the Coulomb interaction, the interaction with the atoms in the target, resolutions of the detectors, and other experimental effects. Given an initial density distribution of molecular coordinates in R space it provides the corresponding distribution of V-space density which can be compared to the experimental data. The estimation of the original R-space distribution and the propagation of the statistical errors from the measurement in V space were performed by a specially developed procedure which has been described elsewhere [47]. The following is a brief description of its application to
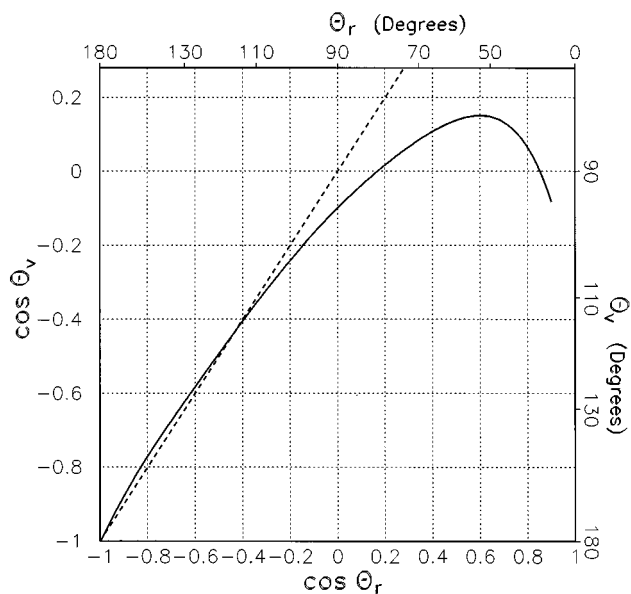

FIG. 3. A mapping of $\cos(\theta_r)$ to $\cos(\theta_v)$ is shown for an ideal Coulomb explosion of NH_2^+. The charge on the nitrogen ion was $q = +3$, and the NH bond length was taken to be $r_e = 1.030$ Å. The dashed curve is the line: $\cos(\theta_r) = \cos(\theta_v)$, shown for comparison.

the present problem. For a deeper insight into this data representation and deconvolution method the reader is referred to Ref. [47].

(1) The V-space bond-angle distribution density function of the measured angle $f(x_v)$ (where $x_v = \cos_v$) was expanded by a set of specially chosen orthogonal functions $f_k'(x_v)$ as

$$f(x_v) = \sum_k [f_k'] f_k'(x_v). \tag{1}$$

The expansion functions, $f_k'(x_v)$ were orthonormal such that

$$\int f_k'(x_v) f_l'(x_v) \, dx_v = \delta_{kl}; \tag{2}$$

therefore, the coefficients $[f_k']$ and their covariance matrix $\text{cov}([f_k'],[f_l'])$ were estimated directly from the data:

$$[f_k'] = \frac{1}{N} \sum_{\alpha=1}^{N} f_k'(x_v^{(\alpha)}) \tag{3}$$

and

$$\text{cov}([f_k'],[f_l']) = \frac{1}{N} \sum_{\alpha=1}^{N} [f_k'(x_v^{(\alpha)}) - [f_k']][f_l'(x_v^{(\alpha)}) - [f_l']], \tag{4}$$

where the summation is on the sample of N measured events. The result is a full functional representation of the data which consists of a relatively small number of coefficients and their correlated errors. In addition, the functions f_k' are modified by an orthogonal transformation which diagonalizes $\text{cov}([f_k'],[f_l'])$. This results in a set of new functions $f_k(x_v)$ and new coefficients $[f_k]$ with uncorrelated errors. This is a faithful representation of the measured data which replaces the more conventional method of representing such data by a histogram.

(2) The distribution of the R-space coordinate $x_r = \cos \theta_r$ was also expanded by another orthonormal set of functions,

$$g(x_r) = \sum [g_k] g_k(x_r), \tag{5}$$

where the coefficients $[g_k]$ were to be found by an iterative procedure. At the starting point of this procedure we assumed that the R-space distribution $g(x_r)$ is equal to the V-space distribution $f(x_v)$.

(3) Given $g(x_r)$ and the theoretical values for the equilibrium bond lengths, the Monte Carlo simulation of CEI was used to compute the corresponding V-space distribution. This process produces an ensemble of simulated molecules in V space which are treated, like in step (1) above, as simulated measured data. It yields a set of coefficients $[\hat{f_k}]$ and a set of corresponding uncorrelated errors. In general, these are not equal to $[f_k]$. Symbolically

$$[g] \Rightarrow \text{simulations} \Rightarrow [\hat{f}]. \tag{6}$$

We also calculated the linear deviations

$$[g] + \delta[g] \Rightarrow \text{simulations} \Rightarrow [\hat{f}] + \delta[\hat{f}], \tag{7}$$

which yields the transformation matrix

$$J_{k,l} = \frac{\delta[\hat{f}_k]}{\delta[g_l]}. \tag{8}$$

(4) Then the R-space distribution function was corrected by

$$\Delta[g] = J^{-1}([f] - [\hat{f}]). \tag{9}$$

and steps (2)–(4) were repeated iteratively a few times (typically three or four times) until convergence was achieved in the sense that $([f] - [\hat{f}])$ was of the order of the experimental statistical error.

(5) *Error propagation.* The functions $g_k(x_r)$ were specially chosen by the use of orthogonal transformations such that the transformation Jacobian J had a diagonal form. As we already emphasized in step (1), the error matrix of the coefficients $[f_k]$ has been diagonalized. Therefore, the propagation of the statistical error to R space could be obtained by simple matrix inversion as in Eq. (9).

The final result of the iterative inversion method was a set of uncorrelated coefficients and their associated errors. Any expectation value of the x_r variable in R space can be extracted from the generated density with the appropriate experimental error. In particular, the R-space density is given by a linear combination of a set of specified orthogonal functions $g_k(x_r)$ with coefficients $[g_k]$ and associated uncorrelated errors $\sigma_{[g_k]}$.

IV. CEI OF H$_2$O$^+$

The molecular ions were produced by electron impact on neutral H_2O in two types of ion sources: a low-energy electron-impact source and a supersonic expansion source with argon as a buffer gas. In the latter case, water vapor was introduced into the ion source reservoir tank in the following manner. The tank was evacuated and then opened to atmosphere through a tube which contained a moist sponge filter. As air was drawn through the tube, it was humidified by the sponge. After this process was complete the tank was filled with 80 psig of Ar. Using the vapor pressure of water, the concentration of H_2O in Ar was estimated to be 0.4%. The ions were then extracted and accelerated to an energy of 4.235 MeV. In these experiments a 0.6 μg/cm^2 (60 Å) Formvar target was used [41].

Figure 4 shows three V-space bond angle probability distributions of H_2O^+ taken with various ion source conditions. The distribution is histogrammed as a function of $x_v = \cos \theta_v$ (rather than θ_v) because the phase space available to the molecule for the bending vibration is singular at $\theta_v = 180°$, and the probability therefore shrinks to zero at that point. For all of the results presented here, the charge of the detected oxygen ion was $q = +4$. However, we also investigated $q = +3$ and $+5$, and verified the insensitivity of the final result (R-space distribution) to the heavy ion charge state. In all cases, the variations with charge state were completely accounted for by the Coulomb explosion kinematics [14].

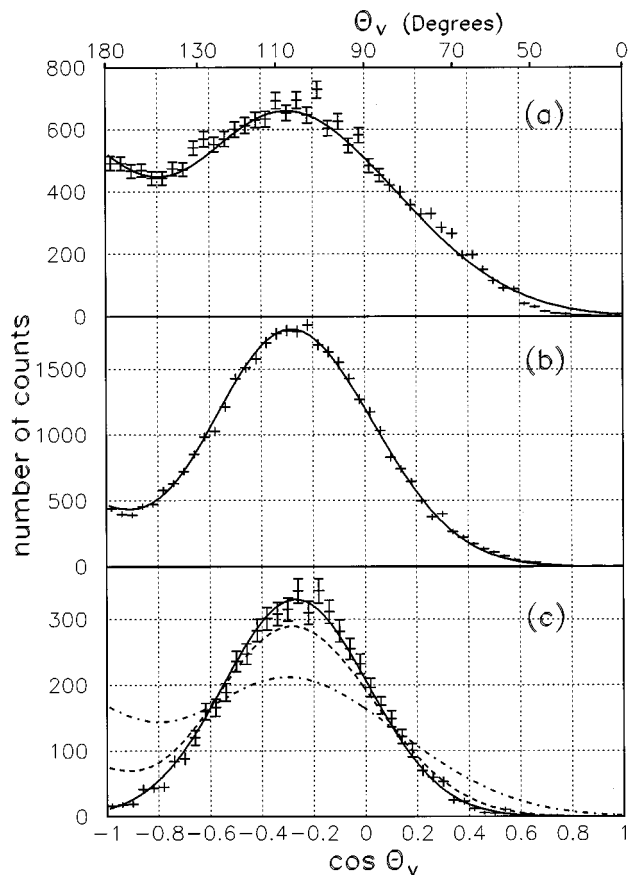The distribution in Fig. 4(a) was obtained using the super-

FIG. 4. The experimental *V*-space probability distributions for the bend angle of H_2O^+ are shown for three different vibrational cooling conditions. The hottest distribution is shown in (a), and the coldest is shown in (c). The solid lines are the fitted analytical distribution functions. In (c) the distribution is compared to (b) (dashed line) and (a) (dash-dotted line) with normalization to the same integral. The data in (b) are reproduced from Ref. [14].

sonic expansion source without electrostatic shielding. As mentioned previously, in the absence of shielding, stray fields created in the interaction region by the electron gun cause ion collisions to occur and heat the beam. The two most prominent features of this distribution are its large width when compared to Figs. 4(b) and 4(c), and the local maximum at $x_v = -1$ ($\theta_v = 180°$).

The distribution in Fig. 4(b) was taken with a modified Duoplasmatron ion source [14]. A retarding grid was installed in front of the filament [36]. This had the effect of producing a narrow electron kinetic-energy distribution with a mean energy comparable to or just above the ionization threshold of the molecule of interest. Since the Franck-Condon factors for a transition from the neutral ground vibrational state of H_2O to the ionic ground vibrational state are extremely favorable ($F_0 = 0.85$, $F_1 = 0.15$, and $F_n = 0$ for $\nu > 1$ [48]), it was expected that this source would produce ions mainly in the ground vibrational state. The distribution in Fig. 4(b) is evidently colder than the one in Fig. 4(a), as can be seen by the lower probability density at 180° and the reduced width of the main peak.

The coldest probability density distribution taken with the shielded supersonic expansion source is shown in Fig. 4(c). The energy of the ionizing electrons was ~ 200 eV. The

stagnation pressure and temperature were ~ 700 Torr and ~ 300 K. In this measurement the electrostatic fields due to the electron gun were shielded and did not affect the expansion. In comparison with Figs. 4(a) and 4(b), there is a dramatic reduction in the probability density at 180° and the width of the distribution is significantly decreased.

Following the discussion in Sec. III A, we used Eq. (1) to create a functional representation of the data. We expanded Eq. (1) by an orthogonal set of functions in the form of Gaussian weighted polynomials $P_n(x_v)$:

$$f_k(x_v) = P_k(x_v)\exp\left(-\frac{(x_v - x_v^0)^2}{2\sigma_v^2}\right). \qquad (10)$$

The fixed parameters x_v^0 and σ_v were chosen to minimize the needed number of functions f_k (see below).

The solid lines in Fig. 4 are results of the fitted distributions using three functions in the expansion. We verified that the contribution of additional terms to the expansion was less than the statistical error. Figure 4(c) compares the properly normalized fits from the three distributions. The reduction in probability density at 180° along with the decrease in width can be understood in terms of the two lowest electronic states of the molecule: the linear $\widetilde{A}^2A_1$ state and the bent $\widetilde{X}^2B_1$ ground state.

The probability distribution $g(x_r)$ for finding the *R*-space H-O-H angle θ_r in the measured ensemble was extracted using the coldest data set and the prescription given above. The coefficients and errors, as well as the definitions of the functions $g_k(x_r)$, are given in Table II. This should enable the reader to reproduce *R*-space distributions together with the corresponding error limits. The resulting *R*-space distribution is presented in Fig. 5 within error limits. The dashed line in Fig. 5 represents the square of the vibrational ground-state wave function associated with the bending motion in the electronic ground state. This theoretical prediction was based on *ab initio* calculations of the potential surface given by Brommer *et al.* [4]. The wave function was obtained using the Hamiltonian by Carter and Handy [23] in terms of internal coordinates. The OH bond lengths were assumed to be constants. The *V*-space distribution function $\hat{f}(x_v)$ that results from the deconvoluted *R*-space distribution is compared to the measured data in Fig. 6. Figure 6(a) presents the distribution function of the measured data within one standard deviation error limits. Figure 6(b) shows the difference between the distribution that is a result of the simulation and the measured distribution in Fig. 6(a). In this representation the measured distribution error limits are described by the shaded curve. This consistency check of the minimization procedure shows very good agreement.

V. CEI OF CH_2^+

The results of the CH_2^+ measurement by CEI have been published recently [22], and we quote here the main results of that work to complete the picture of the XH_2^+ series. The *R*-space distribution is reanalyzed here by the method described above. In addition, the error propagation to *R* space is presented.

Different ion source conditions demonstrated different de-

TABLE II. The bending angle distribution of H_2O^+, CH_2^+, and NH_2^+ is given in the uncorrelated-error representation: $g(x_r) = \Sigma[g_n]g_n(x_r)$. The representation functions are of the form $g_n(x_r) = P_n(x_r)\exp -(x_r-x_r^0)^2/2\sigma_r^2$, with $P_n(x_r) = \Sigma p_k^n x_r^k$. The uncorrelated coefficients $[g_n]$ are listed with the corresponding standard deviation $\sigma_{[g_n]}$ [a]. The fixed parameters σ_r and x_r^0 are also specified.

			H_2O^+		
				p_k^n	
n	$[g_n]$	$\sigma_{[g_n]}$	$k=0$	$k=1$	$k=2$
1	0.2744	0.0047	0.8463	0.015867	-0.90691
2	0.0253	0.0038	0.025915	-1.0616	0.0094236
3	-0.45230	0.00048	-0.36094	-0.040954	-0.55709

$\sigma_r = 0.2490$
$x_r^0 = -0.2885$

			CH_2^+			
					p_k^n	
n	$[g_n]$	$\sigma_{[g_n]}$	$k=0$	$k=1$	$k=2$	$k=3$
1	0.316	0.014	-4.0777	60.199	-176.78	131.14
2	-0.166	0.010	-1.7423	-7.6967	79.116	-85.561
3	0.7522	0.0047	2.1202	-24.310	116.87	-140.55
4	-0.9506	0.00051	-0.54527	-10.0	46.497	-68.129

$\sigma_r = 0.3568$
$x_r^0 = -1$

			NH_2^+		
				p_k^n	
n	$[g_n]$	$\sigma_{[g_n]}$	$k=0$	$k=1$	$k=2$
1	0.304	0.020	4.639	-57.079	111.13
2	0.988	0.010	0.40423	31.56	-121.46
3	-1.2565	0.0014	-1.9546	16.9	-78.674

$\sigma_r = 0.2226$
$x_r^0 = -1$

[a]The error of the distribution function $g(x_r)$ within one standard deviation is given by $(\Delta g(x_r))^2 = \Sigma_n(\sigma_{[g_n]})^2 g_n^2(x_r)$.

grees of cooling [22] of the CH_2^+ molecules. The most efficient cooling was achieved by utilizing the shielded supersonic expansion source with 0.5% CH_4 seeded in Ar buffer gas. The stagnation pressure was ~ 760 Torr, and the energy of the ionizing electrons was ~ 200 eV. The extracted ions were accelerated to an energy of 3.9 MeV and impinged on a $0.6\mu g/cm^2$ Formvar target. The measured angular distribution is presented in Fig. 7 as a function of the V-space coordinate $x_v = \cos\theta_v$. This distribution is of only those events where the carbon ions left the foil with a charge state $q = +3$. These events constituted 57% of the whole data set. Other less populous charge states of the carbon ion were analyzed as well, and showed no statistically significant trends beyond the simple Coulomb force effects [22]. We note that from the raw data shown in Fig. 7 and in view of the previous discussion of Fig. 3, it is evident that the CH_2^+ molecule has a bent equilibrium structure. The solid line in Fig. 7 represents the analytical density distribution fitted to the data. Similar to the H_2O^+ case, we used the expansion in orthogonal functions of the form given by Eq. (10). Here, we used four terms in the expansion and defined $x_v^0 = -1$

($\cos\theta_v^0 = 180°$). The expansion functions and coefficients of the corresponding distribution in R space are presented in Table II. The probability function $g(x_r)$ is shown in Fig. 8. The data show that CH_2^+ is bent in its ground state, though there is significant tunneling through the linear conformation. The theoretical prediction for the rovibronic ground state (dashed line in Fig. 8) shows similar features, though the width is significantly smaller. This distribution was obtained from the *ab initio* potential surface of Ref. [23]. The consistency of the extracted R-space distribution with the data is presented in Fig. 9, where the measured distribution from Fig. 7 is shown within error limits [Fig. 9(a)] and compared to the V-space distribution simulated directly from the revealed R-space distribution [Fig. 9(b)].

VI. CEI OF NH_2^+

In this experiment, cold NH_2^+ ions were created in the terminal of the Dynamitron using the ''cold'' supersonic expansion source. The stagnation pressure of the expansion was ~ 760 torr, and the energy of the ionizing electrons was
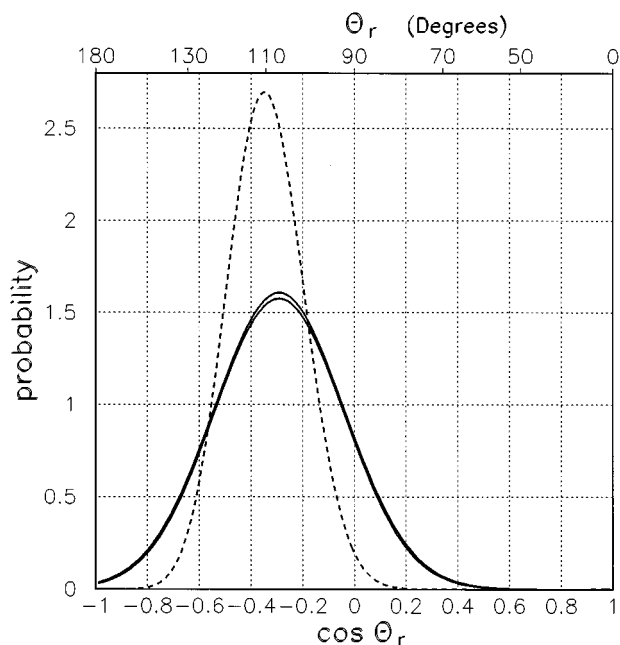
FIG. 5. The extracted R-space distribution of $\cos(\theta_r)$ for H_2O^+ is shown within one standard deviation error limits. The dashed line is a theoretical prediction (Ref. [4]).

~200 eV. For this experiment a mixture of 0.6% NH_3 and 99.4% Ar was used. The ions were extracted from the ion source and accelerated to an energy of 3.9 MeV. The molecules were stripped of their valence electrons by a 0.6-$\mu g/cm^2$ Formvar target.

Again, the ion source was used in two operating modes: shielded and unshielded. As was the case with the previous two molecules, the absence of shielding in the ion source caused relatively high-energy collisions to occur due to stray electric fields in the expansion region. Figure 10 shows the two experimental V-space bond angle probability distributions (points with error bars) of NH_2^+. The data are histogrammed as a function of $\cos\theta_v$. Figure 10(a) shows the "hot" distribution (unshielded source) which is prominently wider than the "cold" distribution in Fig. 10(b). Expansion functions of the form of Eq. (10) were used in this case as for the other molecules. Here three terms were enough to give a statistically sufficient functional representation of the data. The functional representation appears in Fig. 10 as solid lines. In Fig. 10(b) we compare the cold distribution function (solid line) to the hot (renormalized) distribution which is shown with a dashed line.

The probability function $g(x_r)$ for finding the H-N-H angle in the coldest measured ensemble was extracted using the same method employed previously (Fig. 11). The theoretical prediction (dashed line in Fig. 11) is based on the potential given in Ref. [33]. A simulated function $\hat{f}(\theta_v)$ is produced from an initial R-space distribution $R(\theta_r)$, and is directly compared to the data in Fig. 12.

VII. DISCUSSION

As mentioned above, the CEI measurements presented in this study sample observables which differ from those normally probed by traditional spectroscopies, although both
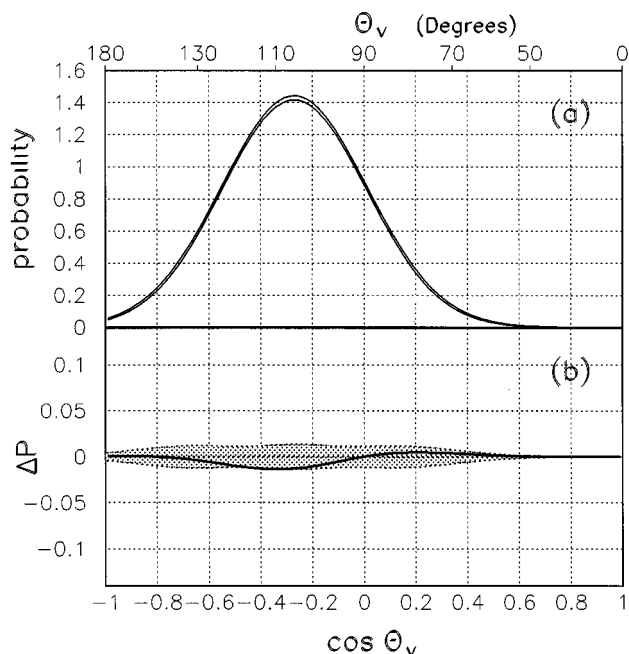

FIG. 6. A comparison between the measured bend angle distribution of H_2O^+ and the result of the Monte Carlo simulation of the extracted R-space distribution. In (a) the distribution function fitted to the experimental data [corresponds to Fig. 4(c)] is plotted within one standard deviation error limits. In (b) the error bands are enhanced and represented by a shaded area. The difference between the two distributions $[\Delta P = f(x_v) - \hat{f}(x_v)]$ appears as a solid line.

study identical quantum systems. The adiabatic approximation supplies a particular model by which one can predict eigenvalues (which can be investigated spectroscopically), as well as eigenfunctions. The latter are closely related to CEI measurements. Below we review the relation of such predictions to the experimental data.

Comparison of the experimental R-space results with the theoretical ground-state densities as shown in Figs. 5, 8, and 11 reveals two trends. First, the most probable bond angles found in the CEI experiments are in fair agreement with the vibrational ground states predictions in *all three* cases examined. A detailed comparison is given in Table III. In contrast, the experimental distributions appear to be *broadened*, showing widths which are systematically larger than theory. To demonstrate how systematic is the broadening, Fig. 13 shows the normalized 0.4 (for example) power of the theoretical distributions versus the measured distributions for all the three species studied. These artificial "agreements" substantiate the regularity of the broadening. Moreover, it suggests that the different broadening in the three studied cases are correlated by some mechanism.

We now consider several possible sources of this apparent widths discrepancy. The most obvious explanation would be thermal or other types of excitation of the ensemble of molecules sampled in the experiment. The low-lying adiabatic potential surfaces of the molecules under study here are shown in Fig. 1. If the cooling method is less effective than is expected, then the measured ensembles of molecular ions would not necessarily be in the vibrational ground state, causing the width of the measured distributions to be larger.
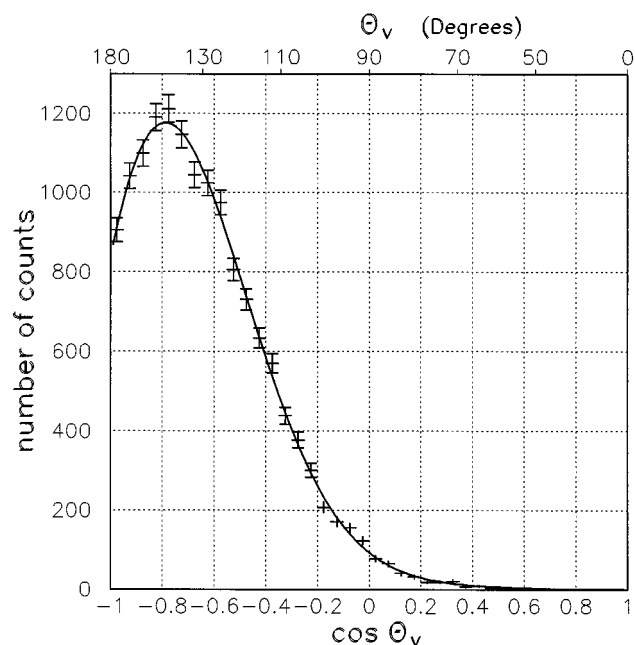
FIG. 7. The experimental *V*-space probability distribution for the bend angle of CH_2^+. The solid line is the fitted analytical distribution function.

FIG. 8. The extracted *R*-space distribution of $\cos(\theta_r)$ in CH_2^+ is shown within one standard deviation error limits. The dashed line is a theoretical prediction (Ref. [23]).

There are several reasons to suspect that this argument is invalid.

(a) A common feature of all of the relevant potentials (Fig. 1) is the strong asymmetry. The potentials are shallower toward the linear conformation, and rise steeply at smaller angles. Consequently, for molecules with bent equilibrium geometries, the presence of excited vibrational states within the measured ensembles should shift the most probable conformations toward that linear shape. This is indeed evident in the measured ''hot'' distributions of H_2O^+ [see, e.g., Fig. 4(c)] and CH_2^+ (see Ref. [22]), where the thermal broadening is asymmetric and shifts the most probable value toward the linear conformation with increasing temperature. A very different behavior is exhibited by the ''cold'' data, and is described below.

The most convincing argument against admixture of vibrationally excited states is found in the CEI measurement of CH_2^+. The deviation of the depth of the observed minimum at the linear conformation (see Fig. 8) from the theoretical curve allows only a gentle admixture of the first vibrationally excited state (for a start, assume only $K=0$ excited states, these are above the barrier). This is demonstrated in Fig. 14, where distributions with different admixtures of the theoretical ground state and the first excited state are compared with the measured data. While the minimum at the linear conformation is filled with any slight admixture of the excited state, the small-angle tail $[\cos(\theta_r) > -0.6]$ hardly broadens. As mentioned above, this is due to the asymmetry of the theoretical potential. Reiterating, the shown admixtures hardly explain the deviation of the observation from the theory on the right side of the peak. In a Renner-Teller case, any rovibrational excitation should admix strongly the linear conformations. Therefore, the above use of the $K=0$ first excited state in the lower branch electronic ground-state potential must be an underestimate of the linear conformation density.
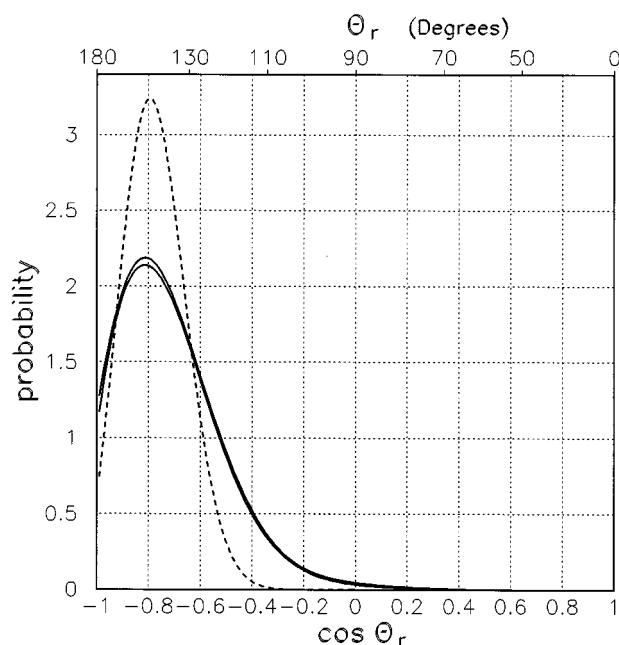
To conclude, the clear and significant measurement of a minimum at the linear conformation points to other reasons for the broadening of the angular distribution than due to a rotational-vibrational excited ensemble.

A similar argument, although less straightforward, is given for the cold NH_2^+ CEI data as follows. Up to an additive constant, the potential energy curve in Fig. 1(c) can be recovered from the the theoretical distribution (the dashed line in Fig. 11) by the use of the Hamiltonian [23]. We refer to this mathematical process as the ''effective-potential recovery.'' If the effective-potential recovery is artificially performed on a theoretical density distribution which is slightly admixed with the first excited state, then the small barrier at the linear conformation starts vanishing. This property is shown in Fig. 15 for different admixtures. Now the effective-potential recovery can be performed on the density given by the CEI data with its associated experimental error. This is shown by the two dashed lines in Fig. 15. As can be seen in this figure, the experimental positive effective barrier at the linear conformation is highly significant, allowing only a small admixture of the first excited state. Yet the experimental effective potential for angles which are smaller than 150° is by far too shallow compared with any of the shown theoretical effective-potentials. This reflects the broad density function which is inconsistent with the possible vibrational excitation within the theoretical potential [33]. Caution should be exercised not to relate the eigenenergies from these artificial effective potentials to spectroscopic results. The use of effective potentials here is only a mathematical tool for comparing the densities. Again, as in the CH_2^+ case, the possible theoretical admixture of excited states which might agree with the data at the linear conformation is far from being consistent with the smaller angles data.

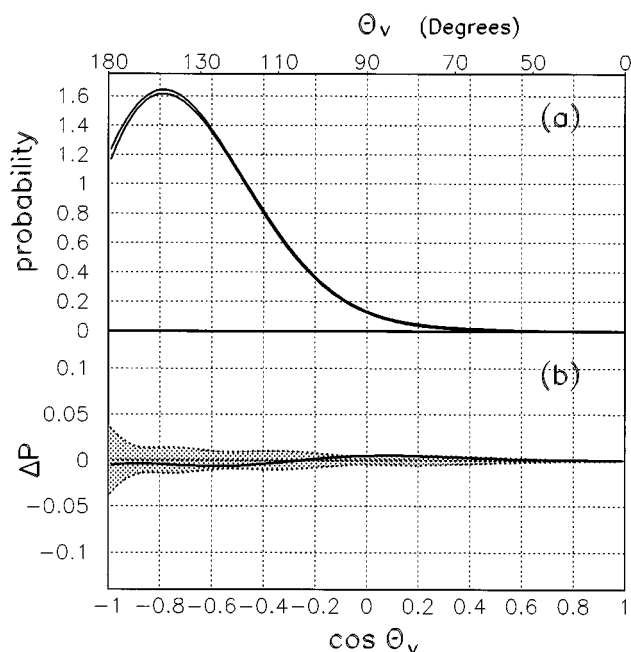For the cold H_2O^+ data, we find that the most probable angle shifts toward smaller angles than the theoretical pre-

FIG. 9. A comparison between the measured bend angle distribution of CH_2^+ and the result of the Monte Carlo simulation of the extracted R-space distribution. In (a) the distribution function fitted to the experimental data (corresponds to Fig. 7) is plotted within one standard deviation error limits. In (b) the error bands are enhanced and represented by a shaded area. The difference between the two distributions $[\Delta P = f(x_v) - \hat{f}(x_v)]$ appears as a solid line.

diction (see Fig. 5). As discussed above, this is in contrast to the expectations of warm distributions. Nevertheless, a best fit to the data with a Boltzmann theoretical vibrational distribution [40] results in a temperature of 2050 K (without resolving the shift of the observed most probable angle).

It is difficult to accept that only CH_2^+ and NH_2^+ ions are cooled by the supersonic ion source, while the H_2O^+ ion comes from the same ion source at ≈ 2000 K for, at least, the following reason. The production of CH_2^+ involves breaking of two hydrogens from CH_4. Similarly, the production of NH_2^+ involves breaking a hydrogen from NH_3. Why should a simple electron ionization of H_2O with a favorable Franck-Condon coefficient for the ground state create such a high excitation?

(b) The *ab initio* potentials (Fig. 1) exhibit major differences in the heights of the barriers at the linear conformations for the different species as well as different positions of the minima. Yet the systematic "spreading" of the widths (Fig. 13) is independent of such details. It is thus improbable that an accidental effective temperature could be found in these three different cases which could meet the regularity of the spreading.

What about the CEI method *per se*? Should we really expect to observe a zero-point vibrational structure in CEI? As we have previously shown [46], the comparatively large-scale nuclear motions in such relatively low-frequency bending vibrations are all well within the resolution limits of these experiments and, under realistic conditions, we should be able to observe zero-point vibrations. Two particularly relevant cases are worth further mention. Previous experiments with He_2^+ and $C_2H_2^+$ both demonstrated good agree-
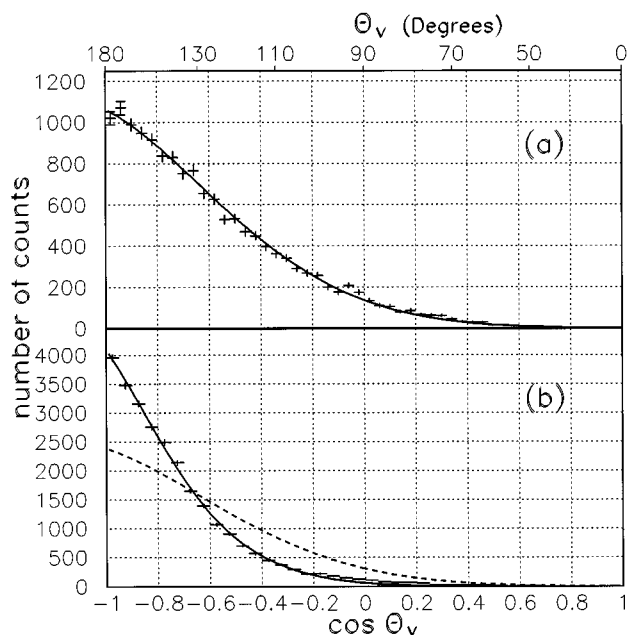

FIG. 10. The experimental V-space probability distributions for the bend angle of NH_2^+ are shown for two different cooling conditions. The hotter distribution is shown in (a), and the coldest one in (b). The solid lines are the fitted analytical distribution functions. The dashed line in (b) is the same as in (a) (normalized to the same integral) for comparison.

ment between CEI results and *ab initio* theory. In the case of He_2^+, it was demonstrated that one could vibrationally cool an ensemble of molecules and observe zero-point vibrations for a high-frequency stretching motion [39,40]. In the case of $C_2H_2^+$ (and the deuterated species), the results showed a linear equilibrium geometry with bending frequencies (i.e.,
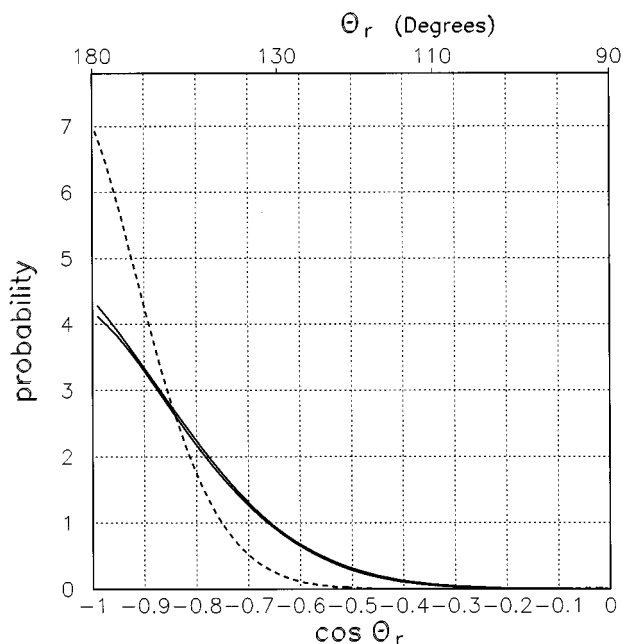

FIG. 11. The extracted R-space distribution of $\cos(\theta_r)$ for NH_2^+ is shown within one standard deviation error limits. The dashed line is a theoretical prediction (Ref. [33]).
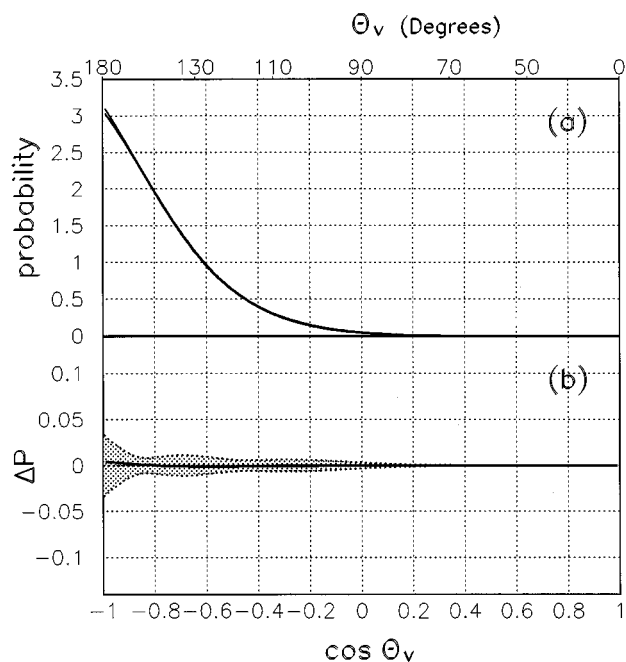
FIG. 12. A comparison between the measured bend angle distribution of NH_2^+ and the result of the Monte Carlo simulation of the extracted R-space distribution. In (a) the distribution function fitted to the experimental data [corresponds to Fig. 10(b)] is plotted within one standard deviation error limits. In (b) the error bands are enhanced and represented by a shaded area. The difference between the two distributions $[\Delta P = f(x_v) - \hat{f}(x_v)]$ appears as a solid line.

distribution widths) in good agreement with theory [14]. Clearly, under some circumstances, the method appears to result in distributions which are consistent with the adiabatic description of structure.

TABLE III. The most probable bending angles θ_m of H_2O^+, CH_2^+, and NH_2^+ as measured by CEI. The theoretical predictions are listed for comparison. All angles are given in degrees.

| | H_2O^+ | |
	CEI	Ref. [4]
$\cos\theta_m$	-0.291±0.003	-0.349 [a]
θ_m	106.9±0.2	110.4 [a]
θ_e		109.3
	CH_2^+	
	CEI	Ref. [23]
$\cos\theta_m$	-0.814±0.004	-0.795 [a]
θ_m	144.5±0.4	142.6 [a]
θ_e		137.9
	NH_2^+	
	CEI	Ref. [33]
$\cos\theta_m$	-1+0.002	-1
θ_m	180.0−3.6	180
θ_e		153.78

[a]The theoretical angle θ_m was obtained from the ground state of the rovibrational Hamiltonian [23] with a potential surface from the cited reference (see Figs. 5, 8, and 11).
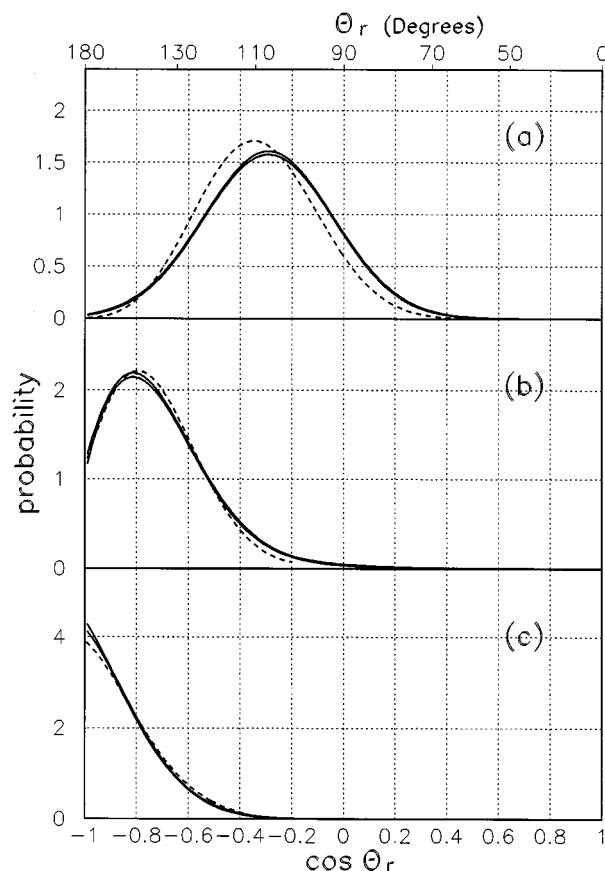

FIG. 13. The R-space distributions (within one standard deviation error limits) of the molecular ions H_2O^+ (a), CH_2^+ (b), and NH_2^+ (c) are compared to the 0.4 power of the ground-state density predicted by theory (renormalized and shown by dashed lines).
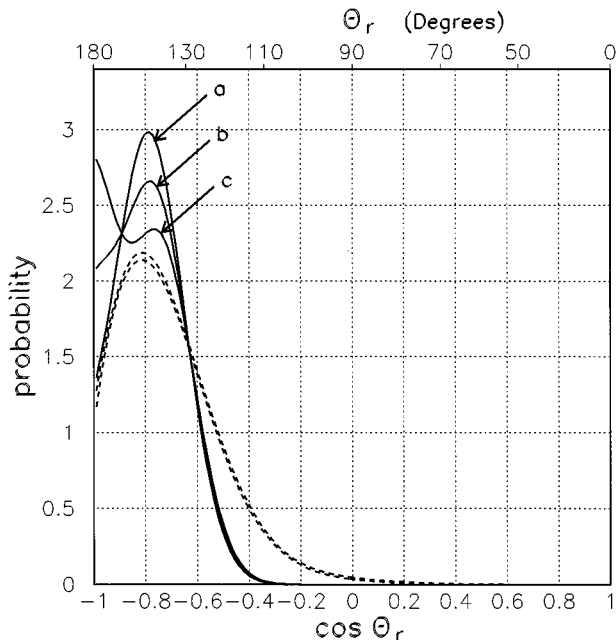

FIG. 14. The same as Fig. 8, but the theoretical curves are given by $(1-\alpha)|\psi_0|^2 + \alpha|\psi_1|^2$. The functions ψ_0 and ψ_1 are the ground and first vibrational eigenfunctions ($K=0$) within the CH_2^+ potential [see Fig. 1 (b)]. (a) $\alpha=0.1$, (b) $\alpha=0.2$, and (c) $\alpha=0.3$.
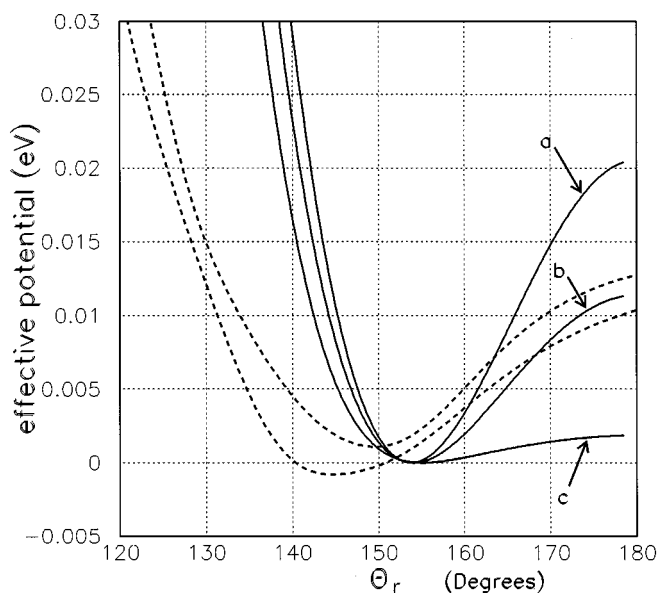
FIG. 15. Effective-potentials recovery (see text) for theoretical densities given by $(1-\alpha)|\psi_0|^2 + \alpha|\psi_1|^2$. The functions ψ_0 and ψ_1 are the ground and first vibrational eigenfunctions ($K=0$) within the NH_2^+ potential [see Fig. 1(c)]. (a) $\alpha=0.00$, (b) $\alpha=0.05$, and (c) $\alpha=0.10$. The dashed lines represent the effective-potential recovery of the experimental density for NH_2^+ with its associated experimental error.

Could our classical trajectory treatment in the simulation of the CEI process be the source of discrepancy? In particular, for the case of H_2O^+, is it conceivable that quantum tunneling effects (e.g., populating the classically unallowed region in V space in Fig. 3) which are ignored in the classical trajectory treatment of the CEI process, could be strong enough to explain the results? A theoretical test of such a possibility was carried out for H_2O^+ [49], with the conclusion that, for this specific case, the quantum effect does not alter the width.

From these considerations, we can only conclude that we observe a true broadening in the measured bond-angle distributions which is inconsistent with the effective Hamiltonian picture generally employed in spectroscopic descriptions. While such treatments are highly successful in describing

rovibrational spectra (and CEI results for fairly rigid linear geometries such as $C_2H_2^+$ [14]), we are apparently mistaken in attempting to extend the resulting adiabatic potential energy surfaces to describe the detailed nuclear densities for these large-amplitude bending motions. These results suggest that a more extensive treatment will be necessary to deduce accurate molecular wave functions for such bent geometries.

VIII. CONCLUSIONS

Apparently, some of the conclusions of the present work are incompatible with the current, well developed, molecular structure theory and gas-phase spectroscopy. Nevertheless, it is important to emphasize those controversial conclusions for the benefit of future scientific discussions which might result a better apprehension of the CEI method and its possible impact on molecular physics.

(1) The most probable angle in each of the three studied molecules agrees fairly well with the available theoretical predictions. This work provides the first experimental determination of the CH_2^+ and NH_2^+ most probable angles. These results were not deduced by the past analysis of gas-phase spectroscopical experiments. It is believed that the information presented here will allow refinement of spectroscopical analysis of these systems.

(2) The CEI measurements presented here yield wider angular distributions than the theoretical predictions of vibrational ground states. Moreover, neither theoretical predictions assuming excited ensembles are compatible with the widths of experimental angular densities presented here. It is important to realize that the CEI method is so far the only direct method for observing such detailed densities.

(3) Although currently we have no understanding of the origin of the wider distribution, it is important to note that there is a common power law that relates the observed distributions to the vibrational ground-state theoretical predictions. Understanding of the origin of this regularity as well as the broadening may elucidate on either the CEI as a method or on our view of molecular structure.

[1] Z. Vager, R. Naaman, and E. P. Kanter, Science **244**, 426 (1989).

[2] P. A. Wehinger, S. Wyckoff, G. H. Herbig, G. Herzberg, and H. Lew, Astrophys. J. **190**, L43 (1974), and references therein.

[3] G. A. Mamon, A. E. Glassgold, and A. Omont, Astrophys. J. **323**, 306 (1987).

[4] M. Brommer, B. Weis, B. Follmeg, P. Rosmus, S. Carter, N. C. Handy, H. -J. Werner, and P. J. Knowles, J. Chem. Phys. **98**, 5222 (1993).

[5] C. R. Brundle and D. W. Turner, Proc. R. Soc. London, Ser. A **307**, 27 (1968).

[6] H. Lew and I. Heiber, J. Chem. Phys. **58**, 1246 (1973).

[7] G. Herzberg and H. Lew, Astron. Astrophys. **31**, 123 (1974).

[8] D. -J. Liu, W. -C. Ho, and T. Oka, J. Chem. Phys. **87**, 2442 (1987).

[9] B. M. Dinelli, M. W. Crofton, and T. Oka, J. Mol. Spectrosc. **127**, 1 (1988).

[10] P. R. Brown, P. B. Davies, and R. J. Stickland, J. Chem. Phys. **91**, 3384 (1989).

[11] T. R. Heut, C. J. Pursell, W. C. Ho, B. M. Dinelli, and T. Oka, J. Chem. Phys. **97**, 5977 (1992).

[12] J. E. Reutt, L. S. Wang, Y. T. Lee, and D. A. Shirley, J. Chem. Phys. **85**, 6928 (1986).

[13] D. Forney, M. E. Jacox, and W. E. Thompson, J. Chem. Phys. **98**, 841 (1993).

[14] D. Zajfman, A. Belkacem, T. Graber, E. P. Kanter, R. E. Mitchell, R. Naaman, Z. Vager, and B. J. Zabransky, J. Chem. Phys. **94**, 2543 (1991).

[15] J. A. Smith, P. Jørgensen, and Y. Öhrn, J. Chem. Phys. **62**, 1285 (1975).

[16] P. J. Fortune, B. J. Rosenberg, and A. C. Wahl, J. Chem. Phys. **65**, 2201 (1976).

[17] C. Jungen and A. J. Merer, Mol. Phys. **40**, 1 (1980).

[18] H. Lew, Can. J. Phys. **54**, 2028 (1976).

[19] W. Reuter, M. Perič, and S. D. Peyerimhoff, Mol. Phys. **74**, 569 (1991).

[20] B. Weis, S. Carter, P. Rosmus, H. -J. Werner, and P. J. Knowles, J. Chem. Phys. **91**, 2818 (1989).

[21] M. Rösslein, C. M. Gabrys, M. -F. Jagod, and T. Oka, J. Mol. Spectrosc. **153**, 738 (1992).

[22] T. Graber, E. P. Kanter, Z. Vager, and D. Zajfman, J. Chem. Phys. **98**, 7725 (1993).

[23] S. Carter and N. C. Handy, Mol. Phys. **52**, 1367 (1984).

[24] R. Bartholomae, D. Martin, and B. T. Sutcliffe, J. Mol. Spectrosc. **87**, 367 (1981).

[25] J. A. Pople and L. A. Curtiss, J. Chem. Phys. **91**, 155 (1987).

[26] D. J. DeFrees and A. D. McLean, J. Chem. Phys. **82**, 333 (1985).

[27] W. Reuter and S. D. Peyerimhoff, Chem. Phys. **160**, 11 (1992).

[28] S. J. Dunlavey, J. M. Dyke, N. Jonathan, and A. Morris, Mol. Phys. **39**, 1121 (1980).

[29] M. Okumura, B. D. Rehfuss, B. M. Dinelli, M. G. Bawendi, and T. Oka, J. Chem. Phys. **90**, 5918 (1989).

[30] Y. Kabbadj, T. R. Huet, D. Uy, and T. Oka, J. Mol. Spectrosc. **175**, 277 (1996).

[31] S. D. Peyerimhoff and R. J. Buenker, Chem. Phys. **42**, 167 (1979).

[32] P. Jensen, P. R. Bunker, and A. D. McLean, Chem. Phys. Lett. **141**, 53 (1987).

[33] V. J. Barclay, I. P. Hamilton, and P. Jensen, J. Chem. Phys. **99**, 9709 (1993).

[34] A. Faibis, E. P. Kanter, L. M. Tack, E. Bakke, and B. J. Zabransky, J. Phys. Chem. **91**, 6445 (1987).

[35] Z. Vager and E. P. Kanter, J. Phys. Chem. **93**, 7745 (1989).

[36] J. E. Hunt, M. Salehpour, A. Ruthenberg, B. Zabransky, R. Amrein, Z. Vager, E. P. Kanter, and D. L. Fishel, Nucl. Instrum. Methods Phys. Res. A **274**, 597 (1989).

[37] E. P. Kanter, P. J. Cooney, D. S. Gemmell, Z. Vager, W. J. Pietsch, and B. J. Zabransky, Nucl. Instrum. Methods **170**, 87 (1980).

[38] E. P. Kanter, D. S. Gemmell, I. Plesser, and Z. Vager, Nucl. Instrum. Methods Phys. Res. **194**, 307 (1982).

[39] T. Graber, D. Zajfman E. P. Kanter, R. Naaman, Z. Vager, and B. J. Zabransky, Rev. Sci. Instrum. **63**, 3569 (1992).

[40] T. J. Graber, Ph.D. thesis, Department of Physics, University of Illinois at Chicago, 1993.

[41] G. Both, E. P. Kanter, Z. Vager, B. J. Zabransky, and D. Zajfman, Rev. Sci. Instrum. **58**, 424 (1987).

[42] S. A. Buzza, E. M. Snyder, D. A. Card, D. E. Folmer, and A. W. Castleman, Jr., J. Chem. Phys. **105**, 7425 (1996); S. Wei, J. Purnell, S. A. Buzza, E. M. Snyder, and A. W. Castleman, Jr., in *Femtosecond Chemistry*, edited by J. Manz and L. Woste (Springer-Verlag, Germany, 1994), p. 449; T. S. Luk, U. Johann, H. Egger, H. Pummer, and C. K. Rhodes, Phys. Rev. A **32**, 214 (1989).

[43] A. Faibis, W. Koenig, E. P. Kanter, and Z. Vager, Nucl. Instrum. Methods Phys. Res. B **13**, 673 (1986).

[44] A. Belkacem, A. Faibis, E. P. Kanter, W. Koenig, R. E. Mitchell, Z. Vager, and B. J. Zabransky, Rev. Sci. Instrum. **61**, 945 (1990).

[45] D. Zajfman, G. Both, E. P. Kanter, and Z. Vager, Phys. Rev. A **41**, 2482 (1990).

[46] D. Zajfman, T. Graber, E. P. Kanter, and Z. Vager, Phys. Rev. A **46**, 194 (1992), and references therein.

[47] J. Levin, D. Kella, and Z. Vager, Phys. Rev. A **53**, 1469 (1996).

[48] W. H. Dibeler, J. A. Walker, and H. M. Rosenstock, J. Res. Natl. Bur. Stand. A **70**, 459 (1966).

[49] H. Feldman and Z. Vager (unpublished).

[50] A. D. Esposti, D. G. Lister, P. Palmieri, and C. D. Esposti, J. Chem. Phys. **87**, 6772 (1987).

[51] A. W. Potts and W. C. Price, Proc. R. Soc. London, Ser. A **326**, 181 (1972).

[52] S. E. Strahan, R. P. Mueller, and R. J. Saykally, J. Chem. Phys. **85**, 1252 (1986).

[53] D. Zajfman, Z. Vager, R. Naaman, R. E. Mitchell, E. P. Kanter, T. Graber, and A. Belkacem, J. Chem. Phys. **94**, 6377 (1991).

[54] T. R. Huet, C. J. Pursell, W. C. Ho, B. M. Dinelli, and T. Oka, J. Chem. Phys. **97**, 5977 (1992).